International Journal of Innovative Technology and Exploring Engineering (IJITEE)
ISSN: 2278-3075 (Online), Volume-9 Issue-4, February 2020

Synthesis and Luminescence Properties of $La_2O_2S:RE^{3+}$ ($RE^{3+} = Ce^{3+}$, Dy^{3+}, Eu^{3+} and Tb^{3+}) Submicron Size Phosphors for Lamp Industry

V. V. Shinde, S. J. Dhoble

***Abstract**: RE^{3+}($RE^{3+} = Ce^{3+}$, Dy^{3+}, Eu^{3+} and Tb^{3+}) doped La_2O_2S phosphors was synthesized by solid state flux fusion method and their down conversion spectral properties were studied as a function different RE^{3+} concentrations and reported in this paper. The solid state flux fusion results in well crystallized hexagonal shaped phosphor particles. The samples were characterized by XRD, SEM, FT-IR photoluminescence (PL) and CIE colour co-ordinates techniques. The lanthanum oxysulphide (La_2O_2S) phosphor doped with Ce^{3+} shows broad band emission with peak at 390 nm and 415 nm when excited at 340 nm excitation. $La_2O_2S:Dy^{3+}$ shows efficient blue and yellow band emissions at 480 nm and 572 nm. $La_2O_2S:Eu^{3+}$ phosphor shows an orange and red emission at 590 nm and 615 nm. Whereas $La_2O_2S:Tb^{3+}$ phosphor shows weak blue emission at 488 nm and strong green 545 nm. The excitation spectra used for the $La_2O_2S:RE^{3+}$ (where $RE^{3+} = Ce^{3+}$, Dy^{3+}, Eu^{3+} and Tb^{3+}) phosphors is in the near UV region extending from 350 to 400 nm, which is characteristics of near UV excited LED. The effect of the RE^{3+} ($RE^{3+}= Ce^{3+}$, Dy^{3+}, Eu^{3+} and Tb^{3+}) concentration on the luminescence properties of $La_2O_2S:RE^{3+}$ phosphors were also studied. The investigated prepared La_2O_2S phosphors may be suitable for a near UV excited W-LED.* ***Keywords**: Oxysulphide, SEM, FT-IR, PL, SSL, CIE.*

I. INTRODUCTION

Global demand for phosphor materials as efficient sources of energy is growing day by day and therefore the development of luminescent materials is the subject of extensive research in the recent years. Particular interest has been focused on inorganic luminescent materials, which have practical applications in almost all devices involving the artificial production of light [1]. In the last decade, there has been a dramatic increase in the number of research on solid-state lighting (SSL) and phosphor materials to generate white light using light emitting diodes (LEDs) as a new light source for general lighting and displays [2].

SSL technology has several advantages over conventional fluorescent lamps such as reduced power consumption, compactness, efficient light output, and longer lifetime.

The conventional white light illumination are mostly composed of blue-emitting InGaN chip and yellow phosphor, typically $Y_3Al_5O_{12}:Ce^{3+}$ (YAG) [3, 4], which exhibits high luminescence efficiency and chemical stability. The combination of blue chip and YAG, however, show a lower colour rendering index (*Ra*) of ~80 due to the lack of red colour contribution. In the second approach, combination of blue LED with two other phosphors emitting red and green light are used. In third approach, three different phosphors which emit red, green and blue light are developed to cover nUV LEDs. The advantage of these LEDs is that they provide large colour area in the CIE diagram and thus enabling the light source more like sunlight. There are only a limited number of phosphor materials that are suitable for this this type of W-LEDs mentioned in third approach.

Lanthanide oxysulphides are known as wide gap (4.6 – 4.8 eV) semiconductors and widely used as efficient phosphorent material host for variety of applications in lighting and display.$La_2O_2S:RE^{3+}$ (Where $RE^{3+} = Ce^{3+}$, Dy^{3+}, Eu^{3+} and Tb^{3+}) is excellent material of current interest owing to their interesting opto-electronic properties. The aim of this work is to investigate and examine the luminescence properties of a $La_2O_2S:RE^{3+}$ (Where $RE^{3+} = Ce^{3+}$, Dy^{3+}, Eu^{3+} and Tb^{3+}) phosphor material with improved photo luminescent properties for lighting applications that can be excited in the near ultraviolet region. The improvement of luminescence intensity through energy transfer from co-doped Ce^{3+} to Dy^{3+}, Eu^{3+} and Tb^{3+} in La_2O_2S host is also discussed in this work.

II. EXPERIMENTAL METHOD

A high temperature solid state flux fusion method was used for synthesising $La_2O_2S:RE^{3+}$ (Where $RE^{3+} = Ce^{3+}$, Dy^{3+}, Eu^{3+} and Tb^{3+}) phosphor. The starting materials are Lanthanum oxide (La_2O_3), Sulphur powder (S) and flux Sodium carbonate (Na_2CO_3), Tri potassium Phosphate (K_3PO_4). Different flux materials such as Sodium carbonate(Na_2CO_3) and Tripotassium Phosphate (K_3PO_4) are used to increase the powder reactivity reaction rate, matrix formation and activator incorporation.

Revised Manuscript Received on February 28, 2020.

***** Correspondence Author
V. V. Shinde, Department of Electronics, Bajaj College of Science, Wardha, India, (email:vvshinde.wda@gmail.com)
S. J. Dhoble*, Department of Physics, RTM Nagpur University, Nagpur-440033, India, (email:sjdhoble@rediffmail.com)

These flux materials, which have melting point below the temperature of phosphor formation and dissolving partially one or both of the reactants, take no part in the solid-state reaction and undergo no reaction with the product [5,6]. Both S and Na_2CO_3 were 30 to 50 weight % and K_3PO_4 was 20 weight % of the total weight.

The dopants were Ammonium Hexanitratocerate $(NH_4)_2Ce(NO_3)_6$) for Ce, Dysprosium oxide (Dy_2O_3) for Dy, Europium oxide (Eu_2O_3,) for Eu and Terbium Oxide (Tb_2O_3) for Tb. The starting materials with dopants in stoichiometric ratio were thoroughly mixed using agate mortar and preheated at 100^OC then fired at 1150 ^0C for 90 min in a muffle furnace. When the furnace was cooled down to room temperature the samples were taken out and washed with distilled water 6 times and finally with a mild hydrochloric acid. The washed powder was subsequently dried and crushed to fine powder using agate mortar.

The formation of La_2O_2S phosphor particle follows the chemical formula:

La_2O_3 +RE_2O_3 +Flux (S+Na_2CO_3 +K_3PO_4) →La_2O_2S: RE + flux residues (Na_2S_x +Na_2SO_4) + gaseous products (HS+SO_4 +CO_2 +O)

The phase purity and structure of the final products of the oxysulphide phosphors La_2O_2S was examined by x-ray powder diffraction using Cu Kα radiation on a BRUKER – analytical x-ray diffractometer. Phosphor morphology was observed by a Geol-6380A scanning electron microscope (SEM). Infrared spectra of the pure La_2O_2S was recorded using a Bruker Fourier transform infrared spectrometer. For the measurement of spectroscopic properties, the excitation and emission spectra for all samples were recorded on Shimadzu make RF-5301PC spectrophotofluorometer using solid sample holder. Emission and excitation spectra were recorded using a spectral slit width of 1.5 nm at room temperature. The co ordinations in the xy-chromaticity diagram are directly calculated from the fluorescent spectra (CIE 1931). All measurements were made at room temperature.

III. RESULTS AND DISCUSSION

A. X-ray Diffraction (XRD)

The comprehensive analysis of phase verification, structural parameters and crystalline structure of La_2O_2S phosphor was carried out by powder X-ray diffraction using diffractometer with CuKα radiation (1.505 A˚) at operating voltage 40 KV, 30 mA and in the range 2θ of 10 – 90 degree, prepared by solid state diffusion method at room temperature . The XRD pattern of the synthesised phosphor material La_2O_2S is as shown in figure 1. It is found that acquired diffraction peaks of the phosphor prepared at 1150˚c are in well agreement with the standard ICDD file No 71-2098. The sample was visually ensured and found to be physically stable (non-hygroscopic) and purely milky white in appearance. The obtained pattern reveals that La_2O_2S powder was formed with no contaminated phases, and implies the complete formation of the homogeneous phosphor material. Reasonably all the diffraction peaks can be indexed to the high crystallinity and high purity of La_2O_2S. The XRD pattern did not indicate the existence of the constituents and other likely phases which are direct authentication of the formation of the phosphor.

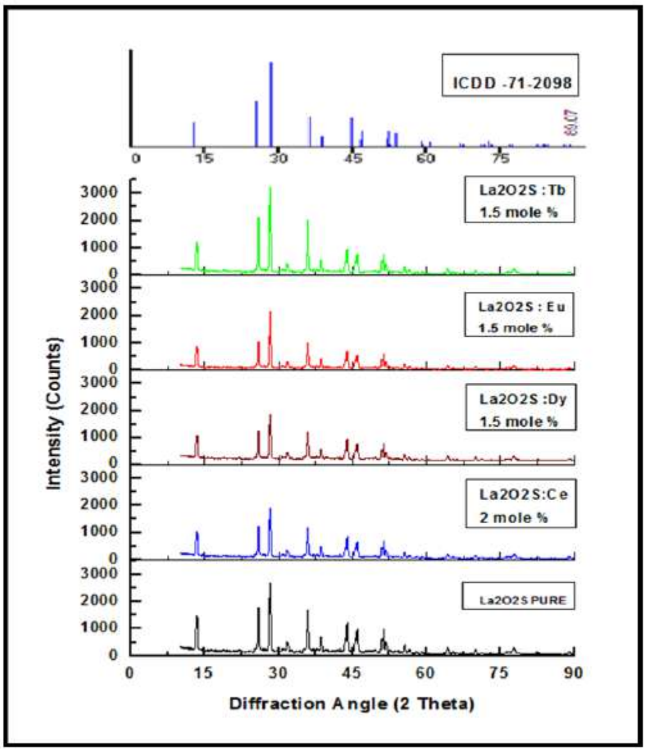

Figure 1: **XRD pattern of La_2O_2S pure and $La_2O_2S:RE^{3+}$ (Where $RE^{3+}= Ce^{3+}$, Dy^{3+}, Eu^{3+}, and Tb^{3+}).**

B. Surface Morphology

Surface morphology of the phosphor was examined by using scanning electron microscopy (SEM, JED-2300) equipped with an energy dispersive spectrometry attached to the JEOL 6380A. SEM images provide the direct information about the size and typical shapes of the prepared samples. SEM micrographs of La_2O_2S and Y_2O_2S phosphors are shown in figure 2. The obtained micrographs show that the particles agglomerate and the average grain size diameter is in the range of 300–800 nm submicron range. It is clearly seen that the sample consists of microspheres with a slight agglomerate phenomenon and is irregularly spherical shaped morphology with a mean diameter of about 300–800 nm. The particle sizes strongly depend on the synthesis methods and synthesis conditions. The particle size and surface morphology which always affect the luminescent properties could be well controlled to improve the luminescent performance.

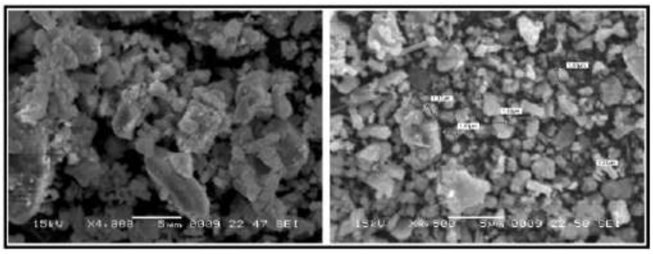

Figure 2: **Scanning electron microscope (SEM) image of synthesized La_2O_2S..**

C. Crystal Structure

Crystal structure of La_2O_2S is shown in figure 3. The symmetry is trigonal and the space group is $P\bar{3}m1$. There is one formula unit per unit cell. The structure is very closely related to the *A*-type rare-earth oxide structure, the difference being that one of the three oxygen sites is occupied by a sulphur atom. Each metal atom seems to be bonded to four oxygen atoms and three sulphur atoms, to form a seven coordinated geometry with the oxygen and the metal in the same plane.

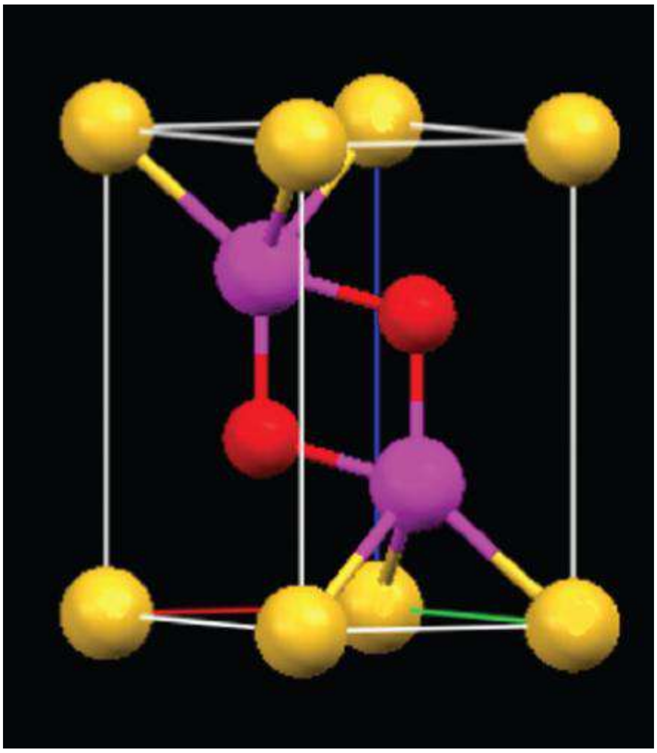

Figure 3: Crystal structure of La_2O_2S. La (Pink), O (red) and S (yellow). (For interpretation of the references to color in this figure legend, the reader is referred to the web version of this article.)

D. FT-IR Analysis

Infrared spectroscopy exploits the fact that molecules have specific frequencies at which they rotate or vibrate corresponding to discrete energy levels. FT-IR spectra shown in figure 4 were recorded in the range of 500 to 4000 cm^{-1} to show the functional groups for pure La_2O_2S sample. The weak absorption band after 3500 cm^{-1} indicates the absorption of water from atmosphere. It is attributed to the stretching vibration of the O–H bond and the bending vibration of H–O–H from water molecules on the external surface of the samples during handling to record the spectra. It is a basic character of lanthanides to absorb water and carbon dioxide when they are exposed to atmosphere. For this reason storing of these compounds away from atmospheric condition is necessary [7–10]. The absorption band of cubic phase La_2O_2S appears at 544, 524 and 517 cm^{-1}. A strong peak at 617 cm^{-1} is related to La-S stretching mode. The weak peak at 880 cm^{-1} can be assigned to S-O stretching group. The weak absorbance at 1454 and 1101 cm^{-1} La-O are symmetric stretching mode.

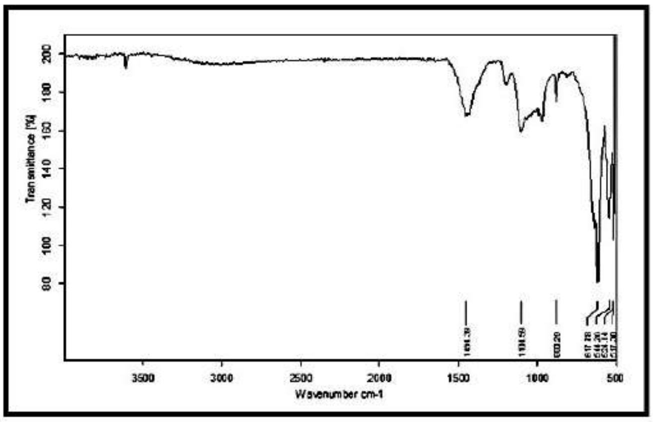

Figure 4: FT-IR spectrum of synthesized La_2O_2S phosphor.

E. PL emission of RE^{3+} in La_2O_2S (Where RE^{3+}= Ce^{3+} , Dy^{3+} , Eu^{3+} , and Tb^{3+})

i) PL emission of Ce^{3+} in La_2O_2S

Figure 5 shows the excitation spectra in the 300–380 nm range and the emission spectra in the 350–500 nm range for samples $La_{2(1-x)}O_2S$: Ce_x (Where X = X = 0.5, 1, 2, 5, and 10 mole %) at room temperature. The excitation spectrum is obtained by monitoring the emission at 415 nm. The broad band is observed at around 340 nm at room temperature. The excitation band at 340 nm is assigned to the lowest 4f–5d transition for Ce^{3+} in the host lattice. A single 4f–5d excitation bands shows that the crystal field might not have split the excited state ($^5D_1$) into more than one component indicating that Ce^{3+} ions occupy one lattice site [11].

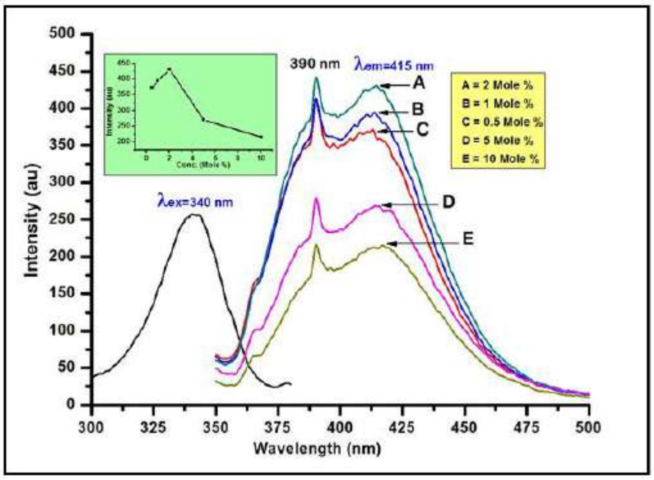

Figure 5: Excitation and emission spectra of synthesized $La_2O_2S:Ce^{3+}$ phosphor.

The PL emission spectra of Ce^{3+} ions in La_2O_2S phosphors with different concentrations under the excitation of 340 nm wavelengths of light is as shown in figure 5. It shows a double humped characteristics with a sharp strong peak at 390 nm and a broad strong peak at 415 nm which are assigned to the 5d-4f transition of Ce^{3+} ions. It is clear that the emission bands correspond to the 5d-4f transition of Ce^{3+} ions. The characteristic emission of Ce^{3+} in the near UV region originates from parity allowed electric dipole transition between excited 5d and ground 4f states.

The 5d orbitals have their energy levels split by crystal effects into at least two sublevels of 5d. Due to spin orbit coupling the lowest sublevels of 5d can be further split into new components, as it is also the case for the ground state level 4f, which splits into the $^2f_{5/2}$ and $^2f_{7/2}$ sublevels. Thus excited state derived from the 5d state is sensitive to the crystal field and is coupled to the lattice vibrations which results in broad band emission rather than line emission. The energy structure of Ce^{3+} is such that localised multiphoton non-radiative relaxation and transfer cross relaxation quenching to other like ions are highly improbable and therefore the 5d luminescence of Ce^{3+} is strong and efficient. The crystal fields play an important role in 5d→4f transitions because 5d levels are outside the Ce atomic nucleus. M. Raukas et al.[12-13] suggested that luminescence efficiency was determined by small but crucial differences on the location of the lowest 5d level relative to the conduction band.

It may be induced by the difference in radius between La^{3+} (R = 103 pm) and Ce^{3+} (R = 100 pm), which will cause the distortion of lattice, the changes of the crystal field and the band gap. All these may cause the Ce^{3+} emission efficiency in La_2O_2S to change. It is also noticed that the peak positions of the emission bands for all Ce^{3+} doped La_2O_2S have not changed.

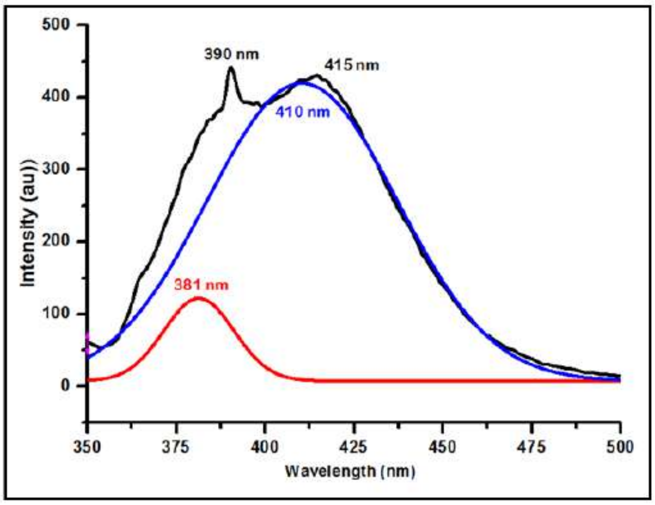

Figure 6: **Gaussian fitted curve for synthesised La_2O_2S:Ce^{3+} phosphor.**

The PL spectrum when further resolved by assuming a Gaussian profile for two emission peaks at 390 and 415 nm, attributed to the transitions of 5d to $^2f_{5/2}$ and $^2f_{2/7}$, respectively, gives the peak at 381 nm and 410 nm as shown in figure 6 . The energy difference between 381 and 410 nm was calculated to be ~1856 cm^{-1}, which is close to theoretical value of ~2000 cm^{-1}. The stoke's shift ΔS (λem=390 nm - λex=340 nm) and (λem=415 nm - λex=340 nm) is found to be 3771 cm^{-1} and 5257 cm^{-1} , respectively. The stoke's shift is due to the strong electron lattice coupling in host. On the basis of configuration coordinate diagram, the excitation band is expanded and therefore the equilibrium of the ground state might have displaced [14].

Various models have been proposed to explain the presence or absence of luminescence. Among them, one-dimensional configuration curve has been most widely used. To illustrate how radiative processes of Ce^{3+} in La_2O_2S phosphor works, a partial electronic energy levels and energetic structure along with configuration co-ordinate diagram are shown in figure 7.

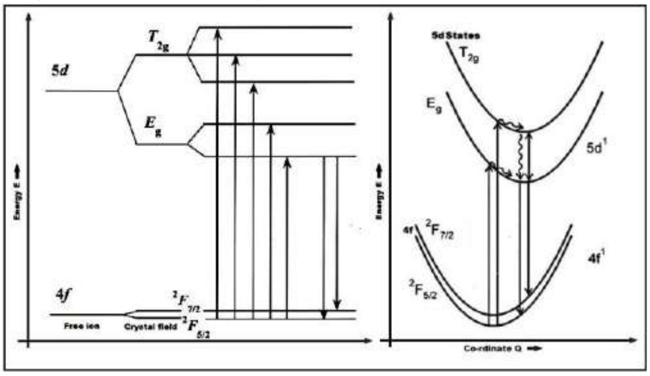

Figure 7: **Schematic illustration of partial energy levels and configurational coordinate diagram of Ce^{3+}.**

In partial electronic structure, the 4f ground state of Ce^{3+} ion is split into $^2F_{7/2}$ and $^2F_{5/2}$ levels due to spin orbit coupling. Its lowest excited state is the 5d band that is easily affected by the crystal field. The crystal field splitting of 5d usually forms 2 to 5 configurations. Ce^{3+} fluorescence is related to an electric dipole 4f→5d transition [15]. The transition is parity and spin allowed. When Ce^{3+} is placed in a crystal, the emission occurs from ultraviolet to visible band depending on the particular compound or host symmetry. It is because the 5d state of Ce^{3+} is strongly affected by three interrelated effects: crystal field splitting (crystal field effect), covalence (nephelauxectic effect) and Stokes shift.[16] Therefore, the luminescence centre is a good candidate as activators in phosphors with the designed excitation and emission wavelengths because luminescence positions can be flexibly adjusted.

In configuration co-ordinate diagram, the potential energy of the luminescent centre in the crystal lattice is plotted as functions of the configuration coordinate Q. The quantity Q represents the distance between rare earth ion and its surrounding ions. Optical transitions are represented vertically on the configuration co-ordinate diagrams, because they occur rapidly compared with nuclear motions, As we can see, ground and excited states take form of parabola potential wells. The two lowest parabolas represent the ground electronic configuration $^4f_1$ by spin–orbit interaction into $^2F_{5/2}$ (the ground state) and $^2F_{7/2}$ (the first excited state). The lowest states of excited electronic configuration $^5d_1$ are represented by two higher parabolas. Electron–lattice interaction in the excited electronic manifold causes the shift of the respective parabolas in the configurational space. In this diagram, the potential energy of the luminescent centre Ce^{3+} is plotted on the vertical axis and the value of single parameter describing the effective displacement of the ion surrounding the activator, Q, is plotted on the horizontal axis. Promotion of the inner 4f electron to the outer 5d states perturbs the surrounding ions, the lattice relaxes, and the potential energy curve changes as shown below in figure 7.

The good adaptability of the position of the 4f–5d absorptions and the corresponding emissions make Ce^{3+} an important ingredient in light emitting materials. The respective excitation and emission pathways are indicated in figure by arrows [17, 18].

ii) PL emission of Dy^{3+} in La_2O_2S

The photoluminescence excitation and emission spectra of the $La_{2(1-x)}O_2S$: Dy_x (Where X = 0.2, 0.5, 1, 1.5, 2 mole %) optoelectronics phosphor at room temperature is shown in figure 8. The excitation spectrum in the range 350 - 400 nm consists of the f-f transition of the Dy^{3+} ion**.** The excitation peaks observed at 351 nm, 367 nm and 388 nm are due to transitions from ground level, $^6H15/2$ to higher energy levels $^4G11/2$, $^4I15/2$, and $^4F9/2$ of Dy^{3+} ion, respectively. Amongst these three near UV excitation peaks, though the emission intensity is larger for λex=351 nm and λex=367 nm as shown in figure 8, we chose 388 nm as excitation wavelength because it is more suitable for solid state lighting [19, 20].

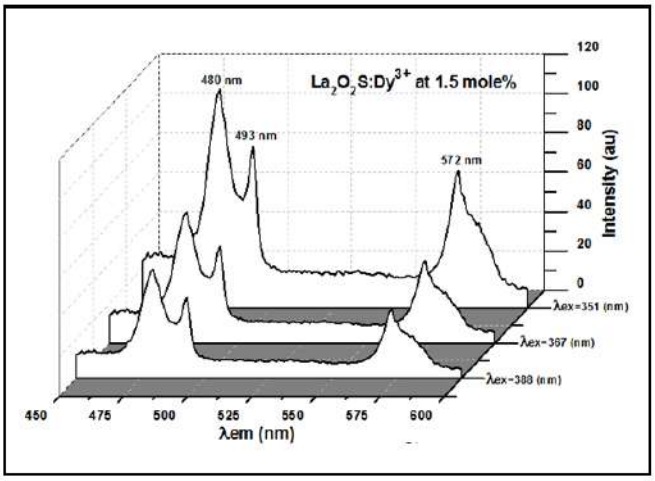

Figure 8: Emission spectra of synthesized La_2O_2S:Dy^{3+} phosphor at 1.5 mole% for various excitation wavelengths.

La_2O_2S:Dy^{3+} phosphor exhibits characteristics emission bands centred at 480 nm and yellow band at 572 nm originating from Dy^{3+} ion under the excitation of 388 nm. Dy^{3+} emission at around 480 nm ($^4F9/2 \rightarrow {}^6H15/2$) is due to magnetic dipole moment and 576 nm ($4F9/2 \rightarrow 6H13/2$) is due to electric dipole moment. The ionic radius of Dy^{3+} (91.2 pm) is much smaller than that La^{3+} (103 pm). Therefore, most of the Dy^{3+} ions may have entered the lattice with few of them located on the surface of the La_2O_2S:Dy^{3+} host crystal due to the porosity of the structure. From the PL spectra it is clear that, energy transfer is possible from the host to the Dy^{3+} activator ions in La_2O_2S:Dy^{3+}host lattice. The inset of figure 9, shows the dependence of the luminescence intensity with the Dy^{3+} concentration. The emission spectrum shape does not vary with the Dy^{3+} concentration but the luminescence intensity changes more significantly. It is found that the emission intensity of Dy^{3+} increases with an increase of dopant ion concentration. It reaches to a maximum value at 1 mole %, and then decreases with an increase of dopant at 2 mole % due to self-quench processes. Such near UV excitation in phosphors host may be helpful for white-LEDs [21 – 24].

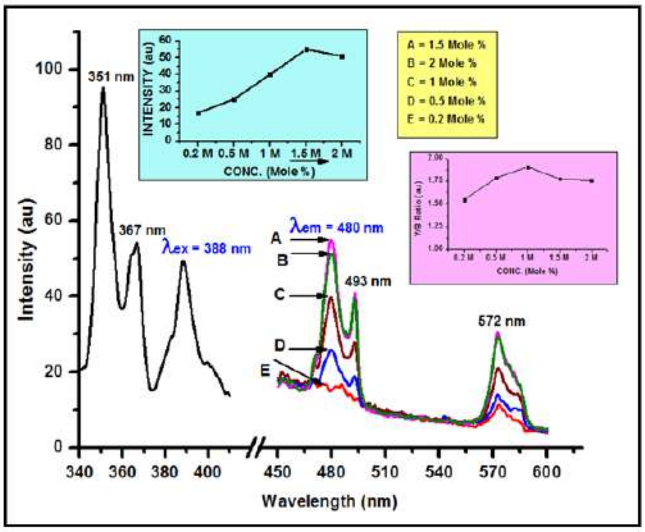

Figure 9: Excitation and emission spectra of synthesised La_2O_2S:Dy^{3+} phosphor.

The emission intensity of yellow to blue (Y/B) ratio is depicted in inset of figure 9. By carefully observing the emission spectra it is found that the emission intensity of yellow to blue (Y/B) ratio is less than 1. This shows that Dy^{3+} ions occupy the site with inversion symmetry predominantly [25].

The partial energy levels and energetic structure and radiative processes in Dy^{3+} are presented in a configurational coordinate diagram in figure 10. In the figure the ^6H and ^6F states of the ground multiplet and the ^4F, ^4I, and ^4G states of the $^4f_9$ electronic configuration, are presented. Under excitation through $^4f_9$ transitions in the Dy^{3+} ion at 388 nm the system can relax nonradiatively to the $^4F_{9/2}$ state and then yield Dy^{3+} emission. The respective emission pathways are indicated in figure by arrows.

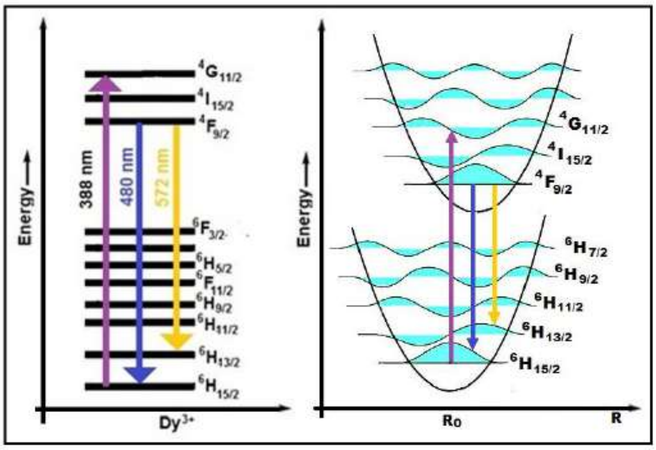

Figure 10: Schematic illustration of partial energy levels and configurational coordinate diagram of Dy^{3+}.

iii) PL emission of Eu^{3+} in La_2O_2S

The PL excitation spectra of $La_{2(1-x)}O_2S$: Eu_x (Where X = 0.2, 0.5, 1, 1.5, 2 mole %) optoelectronics phosphor at room temperature is shown in figure 11. The excitation spectrum at 396 nm is characteristic of W-LED excitation in the near UV range. The sharp excitation peaks between 350 and 400 nm are due to the typical f-f transition of Eu^{3+}. The strongest line absorption in the excitation spectrum is located at 396 nm, which is resulting from the $^7F_0 \rightarrow ^5L_6$ transition [26, 27].

The $La_2O_2S:Eu^{3+}$ phosphor has one sharp orange emission bands at 590 nm and weak bands at 615 nm due to characteristics emission of Eu^{3+} ion, as shown in figure 11, observed due to the $^5D_0 \rightarrow$ $^7F_{i=0,1,2,3,4}$ transitions of Eu^{3+} ions. The emission band at 590 nm is more prominent and corresponds to the magnetic dipole transition ($^5D_0 \rightarrow ^7F_1$) of Eu^{3+} ion whereas the emission band at 615 nm is less prominent and is due to electric dipole transition ($^5D_0 \rightarrow ^7F_2$) of Eu^{3+} ion. These two emission peaks are obtained due to crystal field splitting of $^5D_0$ level to ^7F_j ground state levels. The luminescence spectra of Eu^{3+} ion is slightly influenced by surrounding ligands of the host material because the transition of Eu^{3+} involve only a redistribution of electrons within the inner 4f subshells. The relative intensities of the 590 nm ($^5D_0 \rightarrow ^7F_1$) and 615 nm ($^5D_0 \rightarrow ^7F_2$) emissions are very sensitive to the site that Eu^{3+} ions occupied. As for $La_2O_2S:Eu^{3+}$ particles, the Eu^{3+} ions may have occupied the La ion in host lattice and are at a site with inversion symmetry in the La_2O_2S matrix and thus dominating the emission centred at 593 nm corresponding to the 5D0→7F1 magnetic dipole transition. Thus, La_2O_2S: Eu^{3+} phosphor may be promising candidates for the development of white-LEDs [28 – 33].

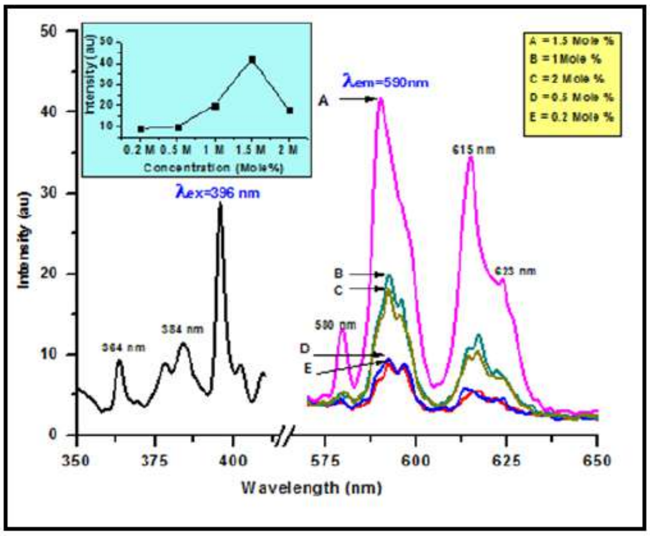

Figure 6: Excitation and emission spectra of $La_2O_2S:Eu^{3+}$ phosphor.

The partial energy levels and energetic structure and radiative processes in Eu^{3+} are presented in a configurational coordinate diagram in figure 12. In the figure the ^7F_J states for J= 0,1,2,3,4,5,6 of the ground multiplet and the excited electronic states $^5D_0$, $^5D_1$, $^5D_2$, $^5D_3$ and $^5L_6$ states of the $^4f_6$ electronic configuration, are presented. Under excitation through $^4f_6$ transitions in the Eu^{3+} ion at 396 nm the system can relax nonradiatively to the $^5D_0$ state and then yield Eu^{3+} emission. The respective emission pathways are indicated in figure by arrows.

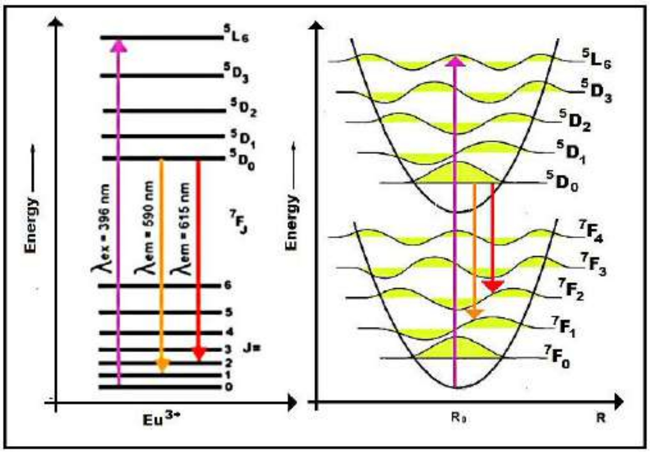

Figure 12: Schematic illustration of partial energy levels and configurational coordinate diagram of Eu^{3+}.

iv) PL emission of Tb^{3+} in La_2O_2S

Figure 13 shows the excitation spectra in the 340–400 nm range and the emission spectra in the 450–650 nm range for samples $La_{2(1-x)}O_2S$: Tb_x (Where X = 0.2, 0.5, 1, 1.5, 2 mole %) at room temperature.

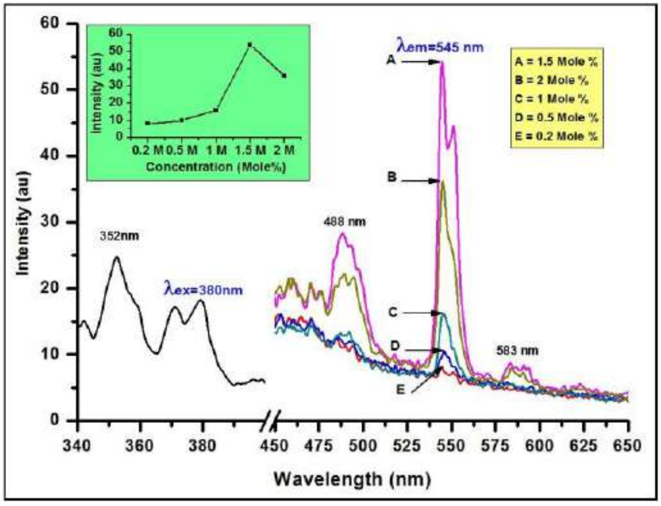

Figure 13: Excitation and emission spectra of $La_2O_2S:Tb^{3+}$ phosphor.

The overall excitation spectrum of Tb^{3+} can be divided into two parts. One, in the wavelength range 220 nm-310 nm comprising of $^4f_8 \rightarrow ^4f_7{}^5d_1$ transitions and other part of the excitation spectrum, in the range 310 nm–500 nm which stands for $^4f_8 \rightarrow ^4f_8$ transitions of the Tb^{3+} ions [34]. There are several excitation peaks in the 340 to 390 nm region corresponding to transitions between $^7F_6$ and the various excited states belonging to the $^4f_8$ electronic configuration of Tb^{3+} ions [35]. The excitation peaks at 352 nm (^{7}F6→^{5}L9), 371 nm (^{7}F6→^{5}G5) and 380 nm (^{7}F6→^{5}G6) due to forbidden 4f-4f transition of Tb^{3+} ion. Though there were significant absorption in the near-UV region and the excitation at 352 nm has highest intensity, we have chosen λex=380 nm as it is more suitable near UV excitation for white LED and therefore La_2O_2S: Tb had potential to be used as near-UV LED phosphors [36].

The emission spectrum of La_2O_2S: Tb is determined by the transitions of electrons from an upper ($^5D_3$) and a lower ($^5D_4$) excited level to the level of the multiplet term ^7F_J (J = 0, 1, 2, 3, 4, 5, 6) levels of the $^4f_8$ configuration [37, 38]. The emission of terbium doped phosphor is mainly in the green due to transitions $^5D_4 \rightarrow ^7F_J$ and the blue emission contributes to the emission from the higher level transitions $^5D_3 \rightarrow ^7F_J$. Figure 13 shows the emission spectra of $La_2O_2S:Tb^{3+}$ phosphors under the excitation wavelength of 380 nm. The emission peaks were found at 488, 545, and 583 nm, which were assigned to the $^5D_4 \rightarrow ^7F_J$ (J = 6, 5, 4) transition of Tb^{3+} ions [9]. As expected, the spectral shift was not observed because the 4f shell of Tb^{3+} was well shielded by 5s and 5p shells. Moreover, the emission from $^5D_3 \rightarrow ^7F_J$ level are quenched by the cross relaxation ($Tb^3(^5D_3) + Tb^3(^7F_6) \rightarrow Tb^3(^5D_4) + Tb^3(7F_1)$) [39 ,40]. The cross relaxation process produces the rapid population of the $^5D_4$ level at the expense of $^5D_3$, resulting in a strong emission from the $^5D_4$ to the ^7F_J level. Generally, the cross relaxation is observed at higher Tb^{3+} concentration, which made good agreement with the results in our case.

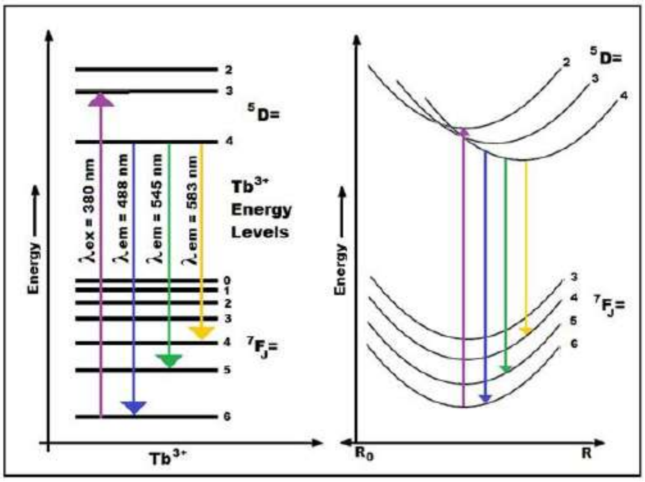

Figure 14: Schematic illustration of partial energy levels and configurational coordinate diagram of Tb^{3+}.

The luminescent mechanism of phosphor is due to competition between the optical activation of Tb^{3+} ions which results in increase of PL intensity and the clustering of Tb^{3+} causes concentration quenching. At lower concentration of concentration, the PL intensity of 545 nm ($^5D4 \rightarrow ^7F5$) and 488 nm ($^5D4 \rightarrow ^7F6$) emissions decreases with increase of Tb^{3+} ion concentration. As the concentration of Tb^{3+} exceed the critical concentration, distance between Tb^{3+} ions become shorter, which cause activator to form pairs and thus results in concentration quenching. The emission intensity reached its optimum doping concentration at about 1.5 mole% in the $La_2O_2S:Tb^{3+}$ phosphors.

The partial energy levels and energetic structure and radiative processes in Tb^{3+} are presented in a configurational coordinate diagram in figure 14. In the figure the ^7F_J states $^7F_3$, $^7F_4$, $^7F_5$, and $^7F_6$ of the ground multiplet and the $^5D_2$, $^5D_3$ and $^5D_4$ states of the $^4f_8$ electronic configuration, are presented. Under excitation through $^4f_8$ transitions in the Tb^{3+} ion at 380 nm the system can relax nonradiatively to the $^5D_4$ state and then yield Tb^{3+} emission. The respective emission pathways are indicated in figure by arrows [41]. Tb^{3+}, the first mechanism is dominant in the luminescent process and the PL intensity increases with the increase in concentration of Tb^{3+}. The inset of figure 13 show the relative PL intensities of 545 nm ($^5D4 \rightarrow ^7F5$) and 488 nm ($^5D4 \rightarrow ^7F6$) emissions under 380 nm excitation. Up to 1.5 mole% concentration of Tb^{3+}ion the PL intensity of 545 nm ($^5D4 \rightarrow ^7F5$) and 488 nm ($^5D4 \rightarrow ^7F6$) emission increases with increase of Tb^{3+} ion concentration above 1.5 mole % .

F. Chromatic Properties

The figure 15 shows the Commission International de l Eclairage (CIE) chromaticity co-ordinates of the prepared phosphor La_2O_2S: RE^{3+} phosphor (Where $RE^{3+} = Ce^{3+}$, Dy^{3+}, Eu^{3+} and Tb^{3+}).The chromatic co-ordinates (X, Y) are calculated using the colour calculator radiant imaging software and are summarized in following table 1.

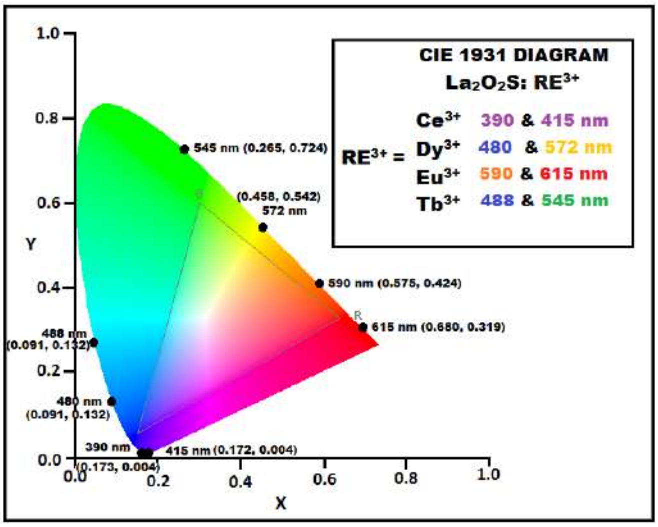

Figure 15: Chromatic graph of La_2O_2S: RE^{3+} phosphor (Where $RE^{3+} = Ce^{3+}$, Dy^{3+}, Eu^{3+} and Tb^{3+}).

G. Luminescence and energy transfer in $La_2O_2S:Tb^{3+}$, Ce^{3+}

In this section, PL characteristics of La_2O_2S phosphor with doubly doped Tb^{3+} and Ce^{3+} is investigated. Energy transfer from Ce^{3+} to Tb^{3+} is also discussed. The Tb^{3+} and Ce^{3+} are two important rare earth ions, which have been used to produce green and blue emission [42]. In addition, Ce^{3+} is also an efficient sensitizer to Tb^{3+}, due to its allowed optical transition from 4f to 5d and broad emission. The broad emission of Ce^{3+} creates high possibility overlapping with the excitation band of Tb^{3+} which gives bright green emission suitable for lighting and display devices.

Emission and excitation spectra of the $La_2O_2S:Ce^{3+}$ and $La_2O_2S:Tb^{3+}$ phosphor is already discussed and shown in

Table I: CIE Co-ordinates of La_2O_2S: RE^{3+} phosphor (Where $RE^{3+} = Ce^{3+}$, Dy^{3+}, Eu^{3+} and Tb^{3+}).

PHOSPHOR	EXCITATION (nm)	STRONG EMISSION (nm)	(X,Y) COORDINATE	COLOUR REGION
La_2O_2S: Ce^{3+}	340	390 415	(0.173, 0.004) (0.172, 0.004)	UV UV
La_2O_2S: Dy^{3+}	397	480 572	(0.091, 0.132) (0.458, 0.542)	Blue Yellow
La_2O_2S: Eu^{3+}	396	590 615	(0.575, 0.424) (0.680, 0.319)	Orange Red
La_2O_2S: Tb^{3+}	380	488 545	(0.091, 0.132) (0.265, 0.724)	Blue Green

figure 5 and 13 respectively. The emission of Ce^{3+} includes emission bands of the transitions of 5d-excited state to $^2F_{7/2}$ and $^2F_{5/2}$ states. The emission spectrum observed in $La_2O_2S:Ce^{3+}$ consist of emission peaking at 390 and 415 nm under excitation wavelength of 340 nm which corresponds to the transitions from ground state of Ce^{3+} to its field splitting levels of $^5d_1$ states [43]. The emission spectra of $La_2O_2S:Tb^{3+}$ phosphor consist of emission peaks at 488, 545, 583 nm, which are assigned to the $^5D_4$ to ^7F_J (J=6, 5, 4) transitions of singly doped Tb^{3+} in La_2O_2S when excited at near UV 380 nm wavelength. Some emissions from $^5D_3$ to ^7F_J (J=5, 4, 3, 2, 1, 0) are also found from 400 to 485 nm in Tb^{3+} singly doped sample [44].

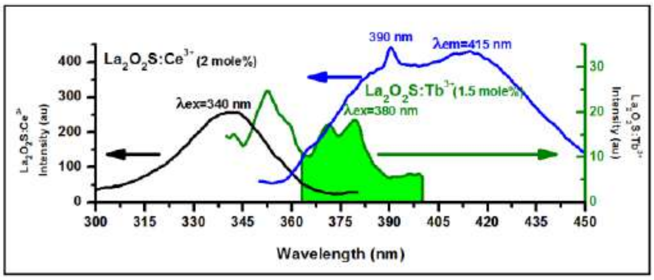

Figure 16: Excitation & Emission spectra of single doped $La_2O_2S:Ce^{3+}$ (2 M%) and Excitation spectrum of $La_2O_2S:Tb^{3+}$ (1.5 M%) showing strong overlap between Ce^{3+} emission and Tb^{3+} absorption in the range 300 to 450 nm.

Energy transfer is controlled by luminescent kinetics, which is affected by energy level, lifetime, distance between co-dopants, etc. One of the dopant is called as activator from where the emission takes place and other is sensitizer, which will improve the luminescence efficiency of activator emission. Ce^{3+} to Tb^{3+} energy transfer process in different host matrices is well known [45, 46]. Broad band emitters are often used to sensitize the luminescence of RE ions. Efficient energy transfer from the broad (i.e., Ce^{3+}) to the narrow-line emitter (i.e., Tb^{3+}) is possible only between nearest neighbours in the crystal lattice and optimal spectral overlap. If the spectral overlap is small, only partial energy transfer is possible.

As shown in figure 16, Ce^{3+} doped sample exhibits broad band emission from 360 - 450 nm, while Tb^{3+} doped sample shows an excitation band ranging from 345 to 400 nm. It means that, there is a strong overlap between Ce^{3+} emission and Tb^{3+} excitation in the range of 360- 400 nm. Therefore, it is expected that an efficient energy transfer can occur from Ce^{3+} to Tb^{3+}.

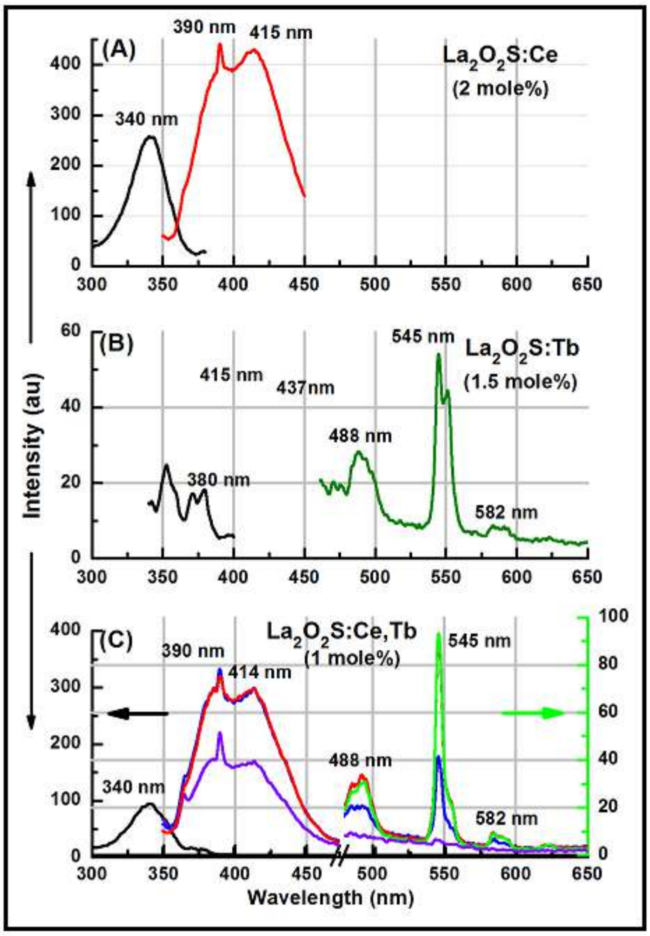

Figure 17: Excitation and emission spectra of the single-doped and co-doped samples, (A) $La_2O_2S:Ce^{3+}$, (B) $La_2O_2S:Tb^{3+}$ and (c) La_2O_2S: $Ce^{3+}\rightarrow Tb^{3+}$.

Figure 17 (A) shows the excitation and emission spectra of $La_2O_2S:Ce^{3+}$ at 2 mole%. Figure 17 (B) shows the excitation and emission spectra of $La_2O_2S:Tb^{3+}$ at 1.5 mole%. Figure 17 (C) depicts the excitation and emission spectra of $La_2O_2S:Ce^{3+}\rightarrow Tb^{3+}$sample. The excitation spectrum is monitored at λem=545nm. The broad excitation band at 340 nm is in agreement with the Ce^{3+} solely doped system.

The emission spectra in Figure 17 (C) indicate the high light output of Tb^{3+} which actually comes from the energy transfer process from Ce^{3+} to Tb^{3+}. The optimal excitation wavelength for Ce^{3+} is 340 nm light excitation but not for Tb^{3+}. In La_2O_2S phosphor, Ce^{3+} not only exhibit the emission at 390 and 414 nm, but also due to energy transfer Tb^{3+} radiates the strong green emission band at 545 nm along with weak emission at 488 and 582 nm. The Ce^{3+} ion first absorbs UV light at 340 nm. An electron is pumped to 5d level, and then non-radiatively relaxes to the lowest component of 5d level finally decaying to $^2F_{5/2}$ and $^2F_{7/2}$ levels by radiative process emitting photons at 390 and 414 nm. As the value of energy level of excited 5d state of Ce^{3+} is close to the $^5D_3$ and other levels of Tb^{3+} ions, the energy transfers from Ce^{3+} to Tb^{3+} ions would have been occurred, promoting it from $^7F_6$ ground state to $^5D_3$ and other levels of Tb^{3+} ion. Then the excited Tb^{3+} ion relaxes, non-radiatively, to the $^5D_4$ levels and gives the strong emission of Tb^{3+} ($^5D_4$-^7F_J). Figure 18 shows schematic energy level diagram indicating $Ce^{3+}\rightarrow Tb^{3+}$ energy transfer in La_2O_2S.

For a better understanding, an energy level model that explains the energy transfer from $Ce^{3+}\rightarrow Tb^{3+}$ is illustrated in figure 18. It shows interaction between the ^5D state of Ce^{3+} and the ^5D state of Tb^{3+}. The $^5D_4 \rightarrow {}^7F_6$ (blue) and $^5D_4 \rightarrow {}^7F_5$ (green) occurs at 488 nm and 588 nm, respectively. As a result, the energy transfer from Ce^{3+} to Tb^{3+} is allowed by the law of conservation of energy. Thus it illustrates that both blue emission and green emission of Tb^{3+} ions could be obtained in the La_2O_2S host, which is the base of multicolour emission under the excitation of UV light in the present system.

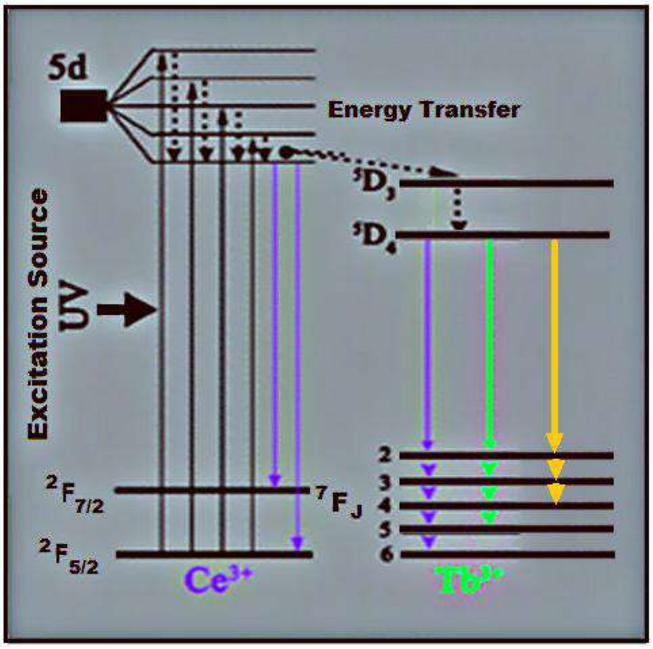

Figure 18: Schematic energy level diagram indicating $Ce^{3+}\rightarrow Tb^{3+}$ energy transfer in La_2O_2S.

The luminescence colours of $La_2O_2S:Ce^{3+}\rightarrow Tb^{3+}$ phosphors excited at 340 nm are characterized by Commission International de I'Eclairage (CIE) chromaticity diagram and is shown in figure 19. The chromaticity coordinate $La_2O_2S:Ce^{3+}\rightarrow Tb^{3+}$ phosphors is calculated to be (0.265, 0.724) for 415 nm and (0.265, 0.724) for 545 nm. The line connecting the chromaticity point passes nearly from white region. It is worthwhile to notice that by combining the emission band of Ce^{3+} ions at blue region and the emission band of Tb^{3+} ions at green region, white light emission may be achieved.

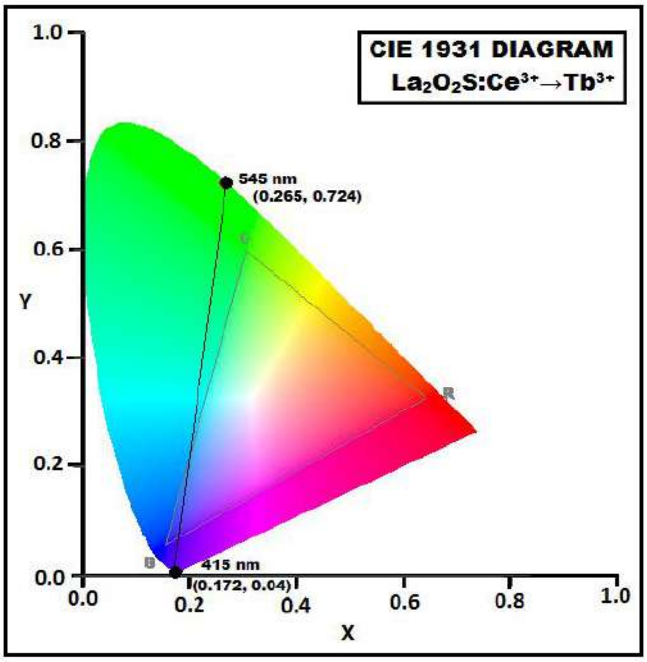

Figure 19: Chromatic graph of $La_2O_2S:Ce^{3+}\rightarrow Tb^{3+}$ phosphors phosphor excited near UV excitation.

IV. CONCLUSION

The $La_2O_2S:RE^{3+}$ (Where RE^{3+} = Ce^{3+}, Dy^{3+}, Eu^{3+} and Tb^{3+}) optoelectronics phosphor has been prepared by the solid state flux diffusion method. PL properties in the near UV and visible region which are characteristics for optoelectronic devices are studied. XRD analysis is carried out to check phase purity of the prepared optoelectronics phosphor. SEM analysis show agglomerates ranging from few microns to a few tens of microns with highly porous morphology of the synthesised phosphor. . FT-IR spectra were recorded to show the functional groups for pure La_2O_2S sample. CIE is carried out to check colour quality of the prepared phosphor. The developed $La_2O_2S:RE^{3+}$ (Where RE^{3+} = Ce^{3+}, Dy^{3+}, Eu^{3+} and Tb^{3+}) phosphor has been excited in near UV range which is desirable characteristics for commercially available W-LED. The developed phosphor emits in the blue, yellow, green and red region. Hence it has potential to be used in phosphor converted LED as a primary colour emitter in 3 band pc-LED or red spectrum enhancer in yellow phosphor converted white LED and therefore our results indicate that prepared phosphor may be a promising candidates for white LEDs. Cross relaxation process led to non-radiative quenching therefore the emission intensity of RE^{3+} ions decreased with increasing amount of doped RE^{3+} ions.

To investigate the energy transfer from Ce^{3+} to Tb^{3+} ions, the emission spectra of $La_2O_2S:Ce^{3+}\rightarrow Tb^{3+}$ phosphors under excitation wavelength 340 nm were measured. The emissions of Ce^{3+} and Tb^{3+} were observed. The intensity of Ce^{3+} emission were found reduced and that of Tb^{3+} increased when compared with emission intensity $La_2O_2S:Ce^{3+}$ and $La_2O_2S:Tb^{3+}$, indicating the energy transfer from Ce^{3+} to Tb^{3+} ions in La_2O_2S host.

REFERENCES

1. P.F.S. Pereira, M.G. Matos, L.R. Avila, E.C.O. Nassor, A. Cestari, K.J. Ciuffi, P.S. Calefi, E.J. Nassar, J. Lumin. 130 (2010) 488.
2. S. Nakamura, T. Mukai, and M. Senoh, Appl. Phys. Lett. 64(13) (1994) 1687.
3. S. Nakamura, MRS Bull, (1997) 29.
4. S. Nakamura and G. Fasol, Springer, (1997) 277.
5. R.C. Ropp, Luminescence and the Solid State, Elsevier, Amsterdam, (1991) 139.
6. P. Dorenbos, Phys. Rev. B 62 (2000) 15640.
7. T. L. Van, M. Che, J. M. Tatibouet, M. Kermarec, J. Catal. 142 (1993) 18.
8. S. Bernal, F. J. Botana, R. Garcia, J. M. Rodriguez-Izquierdo, React. Solids 4 (1987) 23.
9. G. Adachi, N. Imanaka, Chem. Rev., 98 (1998) 1479.
10. S. Bernal, G. Blanco, J. J. Calvino, J. Solid State Chem. 180 (2007) 2154.
11. W. M. Yen, M. Raukas, S. A. Basun, W. Schaik, U. van and Happek, J. Lumin. 69 (1996) 287,
12. M. Raukas, S. A. Basun, W. Schaik Van, W. M. Yen and U. Happek, Appl. Phys. Lett. 69, (1996) 3300
13. G. Blasse and B. C. Grabmaier, Luminescent Materials, (Springer, Berlin, German, (1994), Chap. 3.
14. X. Zhang, B. Park, N. Choi, J. Kima, G. C. Kimc, J. H. Yoo, Materials Letters, 63 (2009) 700.
15. B. F. Aull and H. P. Jenssen Phys. Rev., B 34 (1986) 6647.
16. J. W. H. Van Krevel, H. T. Hintzen, R. Metselaar and A. Meijerink , J. Alloys Compd. 268 (1998) 272.
17. D. Curie, Plenum., (1975), 71.
18. H. G. Drickamer, C. W. Frank, and C. P. Slichter, Proc. Nat. Acad. Sci., 69 (1972) 933.
19. M. Jayasimhadri, B. V. Ratnam, K. Jang, H. S. Lee, B. J. Chen, S. S. Yi, J. H. Jeong, L. R. Moorthy, J. Am. Ceram. Soc. 93 (2010) 494.
20. Q. Su, J. Lin, B. Li, J. Alloys Compd., 225 (1995) 120.
21. W. X. Kuang, Y. N. Fan, K. W. Yao, Y. Chen, J. Solid State Chem. 140 (1998) 354.
22. A. N. Yerpude, S. J. Dhoble, Journal of Luminescence 132 (2012) 2975.
23. D. Marrero-Lopez, P. Nunez, M. Abril, V. Lavin, U.R. Rodriguez-Mendoza, V.D. Rodriguez, J. Non-Cryst. Solids 345 (2004) 377.
24. Z. L. Wang, H. B. Liang, L. Y. Zhou, J. Wang, M. L. Gong, Q. Su, J. Lumin. 128 (2008) 147.
25. X. X. Zhao, X. J. Wang, B. J. Chen, Q. Y. Meng, B. Yan, W. H. Di, Opt. Mater. 29 (2007) 1680.
26. D. Ananias, M. Kostova, F. A. Almeida Paz, A. Ferreira, L. D. Carlos, J. Klinowski, J. Rocha, J. Am. Chem. Soc. 126 (2004) 10410.
27. S. Shionoya,W. M. Yen, Boca 303 Raton, (1999) 190.
28. H. Wang, M. Yu, C. K. Lin, J. Lin, J. Colloid and Interface Sci. 300 (2006) 176.
29. K. N. Shinde, S. J. Dhoble, Animesh Kumar, Physica B 406, (2011), 94.
30. I. M. Nagpure, V. B. Pawade and S. J. Dhoble, Luminescence ,25 (2010) 9.
31. P. S. Thakre, S. C.Gedam, S. J.Dhoble , R. G.Atram doi:10.1016/j.jlumin 06(2011)50.
32. A. N. Yerpude, S. J. Dhoble, Journal of Luminescence, 132 (2012) 1781.
33. Y. D. Huh, J. H. Shim, Y. Kim, Y. R. Do, J. Electrochem. Soc. H57 (2003) 150.
34. Z. Ren, C. Tao, H. Yang and S. Feng, Mater. Lett. 61 (2007) 1654.
35. C. H. Lu, S. V. Godbole, M. Qureshi, Jpn. J. Appl. Phys. 45(4A) (2006) 2606.
36. I. M. Nagpure, K. N. Shinde, S. J. Dhoble, A. Kumar, J. Alloys and Comp., 481 (2009) 632.
37. A. M. Amiryan, A. M. Gurwich, R. V. Ktomina, Journal of Applied Spectroscopy 27 (1977) 468.
38. G. Blasse, B. C. Grabmaier, Luminescent Materials, Springer, Berlin, Heidelberg, (1994).
39. R. P. Rap, J. Electrochem. Soc., 150 (2003) H165 401
40. H. Lai, A. Bao, Y. Yang, Y. Tao, H. Yang, Y. Zhang, L. Han, J. Phys. Chem. C 112 (2008) 282.
41. J. Liao, B. Qiu, H. Lai, H. J. Lumin., 129 (2009) 668.
42. H. Matsukiyo, H. Yamada, Extended Abstracts, (1997) 315.
43. B. Huttl, U. Troppenz, K. O. Velthaus, C. R. Ronda, R. H. Mauch, J. Appl. Phys. 78 (12) (1995) 7282.
44. K. S. Sohn, Y. Y. Choi, H. D. Park, Y. G. Choi, J. Electrochem. Soc., 147 (6) (2000) 2375.
45. S. D. Cheng, C. H. Kam, S. Buddhudu, Mater. Res. Bull., 36 (2001) 1131.
46. J. L. Sommerdijk, J. M. P. J. Vestegen, J. Lumin., 9 (1974) 415.

AUTHORS PROFILE

V. V. Shinde is presently working as Associate Professor & Head, Department of Electronics in Bajaj College of Science, Wardha, Maharashtra. He obtained his Ph. D. from R.T.M. Nagpur University, Nagpur. He has 33 years of teaching experience. He has 7 national and international research papers to his credit.

Prof. Sanjay J. Dhoble, is presently working as Professor in Department of Physics, RTM Nagpur university, Nagpur. He obtained his Ph.D. degree in 1992 in Solid State Physics from RTM Nagpur university, Nagpur.. He has 28 years of teaching and 27 Years of Research Experience. He worked on the synthesis and characterization of solid-state lighting materials, development of radiation dosimetry phosphors using thermo luminescence technique and utilization of fly ash. Dr. Dhoble published/filed 16 patents and more than 552 research papers published in Scopus indexing journals. His h-index is 30 and 5209 citations on Scopus. Dr. Dhoble successfully guided 53 students for Ph.D. degree. He authored following books:

1. Principles and applications of organic light emitting diode (Publisher: Elsevier)
2. Nanomaterials for Green Energy (Publisher: Elsevier)
3. Spectroscopy of Lanthanide Doped Oxide Materials (Publisher: Elsevier)
4. Phosphate phosphors for solid state lighting (Publisher: Springer)
5. Phosphors for energy saving and conversion technology (Publisher:Taylor & Francis Group)
6. Phosphors: Synthesis and Applications (Publisher: Pan Stanford).

Dr. Dhoble is Editor of Luminescence: The Journal of Biological and Chemical Luminescence, John Wiley & Sons Ltd. Publication (Impact Factor: 1.691). He is also recipient of India's Top Faculty Research Award-2018 by Careers 360, for the top ten researchers in India in Physics on the basis of research papers published in Scopus research database in session 2017-2018, on 20th March 2018. His ORCID Id: 0000-0002-4249-8228.